Electronic Structures of Novel Tetrasilyl-Substituted Ethylenes: 5,5,6,6,11,11,12,12-Octaethyl-5,6,11,12-tetrasilanaphthacene and 1,1′-Bis(3,4-benzo-2,2,5,5-tetraethyl-2,5-disilacyclopent-3-enylidene)

Kazuyoshi Tanaka,* Takao Yoshii, and Akihiro Ito

Department of Molecular Engineering, Graduate School of Engineering, Kyoto University, Sakyo-ku, Kyoto, 606-8501, Japan

Mitsuo Ishikawa and Akinobu Naka

Department of Chemical Technology, Kurashiki University of Science and the Arts, 2640 Tsurajima, Nishinoura, Kurashiki, 712-8505, Japan

Mamoru Fujitsuka, Akira Watanabe, and Osamu Ito

Institute for the Chemical Reaction Science, Tohoku University, Katahira, Aoba-ku, Sendai, 980-8577, Japan

Yoichi Matsuzaki

Advanced Technology Research Laboratories, Nippon Steel Corporation, 3-35-1 Ida, Nakahara-ku, Kawasaki, 211-0035, Japan

Received: October 1, 1998

Electronic structures of the two structural isomers of novel tetrasilyl-substituted ethylenes, 5,5,6,6,11,11,-12,12-octaethyl-5,6,11,12-tetrasilanaphthacene (**1**) and 1,1′-bis(3,4-benzo-2,2,5,5-tetraethyl-2,5-disilacyclopent-3-enylidene) (**2**), were studied from the viewpoint of electronic effect occurring from geometrical difference in the vicinity of the tetrasilylethene moiety. Characteristic weak bands at 350 (**1**) and 403 (**2**) nm of the absorption spectra in solution were attributed to the σ(HOMO) → π*(LUMO) transition on the basis of the quantum chemical configuration interaction (CI) calculations by the semiempirical INDO/S model and ab initio Hartree−Fock theory. Moreover, the large bathochromic shift of 53 nm between **1** and **2** could be ascribed to the raising of the HOMO of **2**, as is supported by cyclic voltammetry measurements: the small Si−C−Si bond angle of the tetrasilylethene moiety destabilizes the HOMO energy of **2** compared with that of **1**.

Introduction

The electronic effect of silicon-containing substituted groups on carbon-based π-systems has been an important paradigm in organosilicon chemistry since the discovery of the $\sigma-\pi$ conjugation in phenyldisilanes.[1] Of these organosilicon compounds, tetrasilyl-substituted ethylene is undoubtedly one of the simplified benchmark systems. Sakurai et al. synthesized and investigated a variety of tetrasilylethenes from the viewpoint of overcrowded olefins.[2] The compounds exhibit a weak absorption band at around 350 nm together with the strong $\pi-\pi$* transitions in their UV−vis spectra, and as expected from the bulky silyl groups, most of them take a twisted conformation of the C═C double bond. As is well-known from basic molecular orbital (MO) theory, the torsion of the two methylene moieties causes a decrease in the highest occupied MO (HOMO) (π)−lowest unoccupied MO (LUMO) (π*) gap, leading to the long-wavelength absorption. However, more recently, a series of untwisted tetrasilylethenes showing absorption behavior similar to that of the twisted compounds were synthesized.[2d,3] Moreover, in di- and trisilyl-substituted ethylenes,[4] a bathochromic shift of the lowest-energy absorption band was observed in association with their number of silyl substituents.[3a] This indicates that the silyl substituents on an olefin cause the shift of the absorption to longer wavelength.

These experimental findings can be explained by the MO theoretical consideration of model compounds,[5] as shown in Figure 1. In the case of ethylene, the next HOMO ((HO-1)-MO) is of π-type parallel to the molecular plane. However, this MO increases σ-character as silyl groups are substituted. In addition, the raising of the (HO-1)MO level occurs because of successive replacement of hydrogens by silyl groups, and in the tetrasilylated ethylene, the HOMO (π) and (HO-1)MO (σ) energy levels are finally inverted. On the other hand, the LUMO (π*) energy level is lowered with an increase in the silyl substitution. This is clearly ascribed to pseudo-π-conjugation of C−Si bonding. As a result, it is reasonably understood that an electronic absorption at the longest wavelength is achieved in the tetrasilyl-substituted ethylene.

Herein, it is interesting to extend the above-mentioned tetrasilylethene system into one-dimensional polymer systems in which the ethene moieties are directly linked by two silyl groups as shown in Figure 2. These silicon−carbon unsaturated polymers are classified into three types according to their arrangement among the ethene moieties and the silyl groups: (a) the ladder arrangement with parallel C═C rungs, (b) the

10.1021/jp983933e CCC: $18.00
Published on Web 02/06/1999

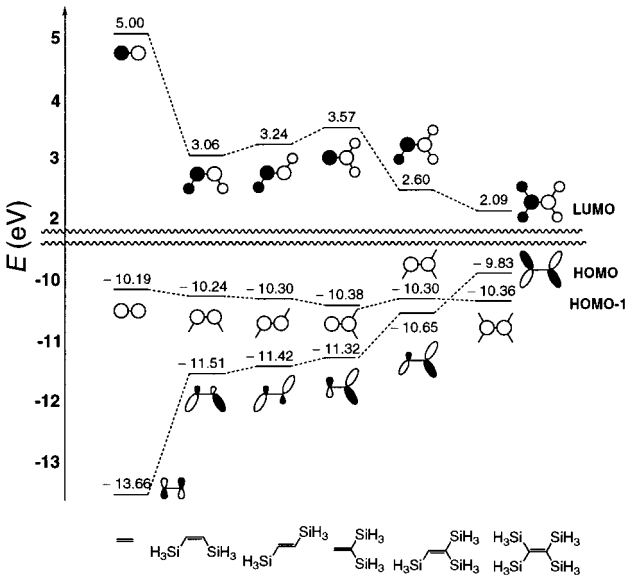

Figure 1. Relative energy levels of the (HO-1)MO, HOMO, and LUMO for ethylene and several silyl-substituted ethylenes based on the RHF/6-31G*//RHF/6-31G* level calculation.

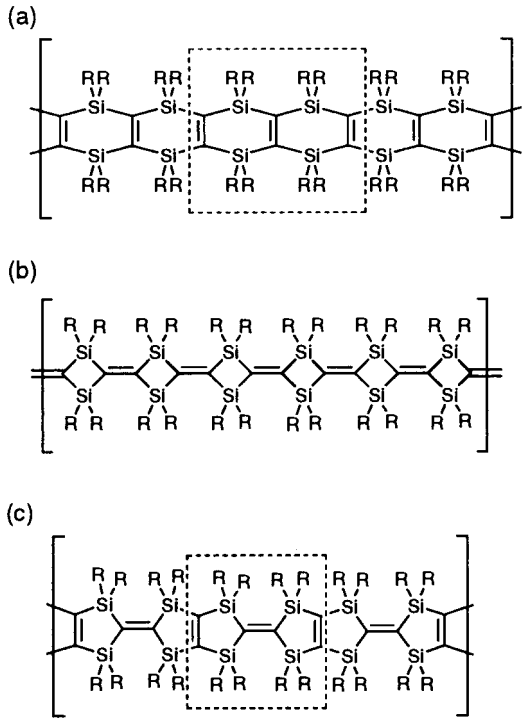

Figure 2. Three types of tetrasilylethene-based polymers: (a) "ladder" arrangement; (b) "chain" arrangement; (c) "hybrid" arrangement of (a) and (b).

chain arrangement, and (c) the hybrid arrangement of (a) and (b). Recently, Naka et al. have synthesized model compounds **1** and **2** corresponding to (a) and (c), respectively.[6] These

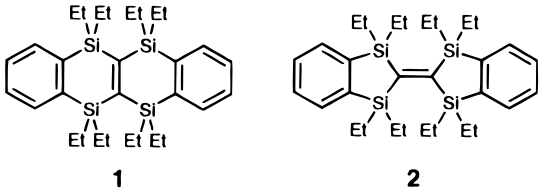

novel compounds exhibit an absorption behavior analogous to

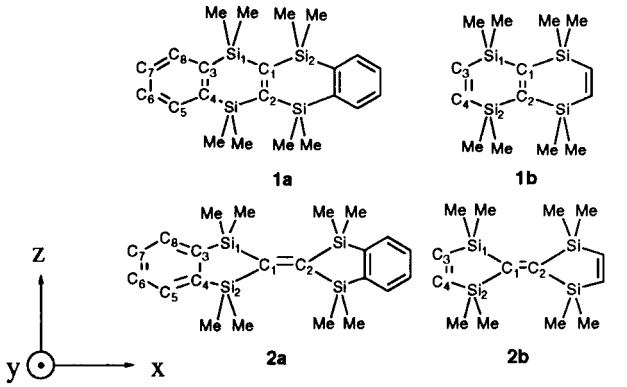

Figure 3. Molecular structures of model compounds **1a**, **2a** **1b**, and **2b** with the coordinate axes employed.

that of the tetrasilylethenes, as will be described in a later section of this paper. Interestingly, in the lowest-energy absorption band around 350 nm, compound **2** showed a large bathochromic shift of 53 nm relative to **1**. This shift is worth investigating because these two compounds are only structural isomers.

In this paper we report the electronic structures of novel tetrasilyl-substituted ethylenes **1** and **2** by both experimental and theoretical investigations. Absorption and emission spectra of **1** and **2** were measured in order to obtain information about their lowest exited states. In addition, the electrochemical properties of **1** and **2** were examined with the use of cyclic voltammetry (CV). Furthermore, we performed semi- and nonempirical MO calculations of the related model compounds **1a**, **2a**, **1b**, and **2b**, as illustrated in Figure 3. Finally, we discuss the specific electronic effect caused by the structural difference between **1** and **2** on the observed bathochromic shift.

Experimental Section

Samples of **1** and **2** were synthesized by heating of 3,4-benzo-1,1,2,2-tetraethyl-1,2-disilacyclobut-3-ene with bis(trimethylsilyl)acetylene in the presence of a $Ni(PEt_3)_4$ catalyst in a sealed glass tube. The detailed conditions are reported in the literature.[6]

UV−vis spectra were recorded on a Shimadzu UV-2200 spectrometer. The CV measurement was performed with a combination of a Hokuto-Denko HA-305 potentiostat, an HB-104 function generator, and a Yokogawa 3025 *XY* recorder with a three-electrode cell using Pt wires as the working and the counter electrodes and an Ag/0.01 M $AgNO_3$ (MeCN) as the reference electrode in a solution of 0.25 mM of **1** (or **2**) and 0.1 M *n*-Bu_4NClO_4 in MeCN (25 °C, scan rate of 100 mV s^{-1}). The observed potential was corrected with reference to ferrocene added as an internal standard after each measurement. Fluorescence spectra were measured with a Hitachi H-850 spectrofluorometer.

Method of Calculation

The geometries of **1a** and **2a** were optimized by the MNDO AM1 (modified neglect of diatomic overlap, Austin model 1) method.[7] To obtain the absorption wavelength and oscillator strength, the singly excited configuration interaction (SECI) calculations were performed using the spectroscopic version of the intermediate neglect of differential overlap (INDO/S-CI) method.[8] The parameters adopted were those of the CNDO/S (the spectroscopic version of complete neglect of differential overlap) method[9] with the exception of the Slater−Condon parameters for the one-center exchange integrals.[10] The two-center electron repulsion integrals were evaluated by the Nishimoto−Mataga formula.[11] For the more simplified model

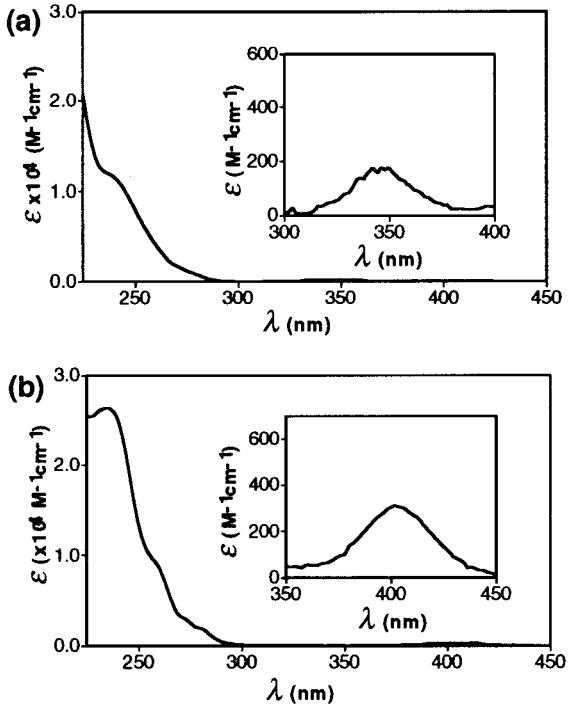

Figure 4. UV−vis spectra of (a) **1** and (b) **2** in cyclohexane at room temperature. The inset shows the enlargement of the lowest-energy absorption band.

TABLE 1: UV−Visible Spectral Data of 1 and 2 (T = 298 K; Cyclohexane Solution)

compd	λ_{max} (nm)	ϵ (M^{-1} cm^{-1})
1	237 sh	12000
	271 sh	1600
	278 sh	900
	350	170
2	235	26000
	258 sh	9700
	272 sh	3000
	280 sh	2000
	403	290

compounds **1b** and **2b**, the ab initio Hartree−Fock calculations were carried out with the 6-31G* basis set.[12] Moreover, the SECI (CIS/6-31G*) calculations were performed with the same basis set at the RHF/6-31G* optimized geometries. All the calculations were carried out with the modified version of CNINDO program[13] and the Gaussian 94 package of ab initio MO programs.[14]

Results and Discussion

Absorption Spectra. As shown in Figure 4, the UV−vis spectra of **1** and **2** in cyclohexane at 289 K had essentially the same features, showing a weak band at 350 and 403 nm, respectively. Moreover, in **2**, a strong absorption band was observed at 235 nm in addition to three shoulder bands in the range 250−300 nm. On the other hand, only three shoulder bands were measured in **1**. The observed absorption wavelength and molar extinction coefficients are summarized in Table 1. It is seen that each absorption wavelength of **2** shows a bathochromic shift compared to that of **1**. In particular, the difference between the longest absorption wavelengths of **1** and **2** was estimated to be 53 nm. The lowest-energy transitions of **1** and **2** did not show the so-called external heavy atom effect in a variety of halogen-containing solvents[15] within experimental

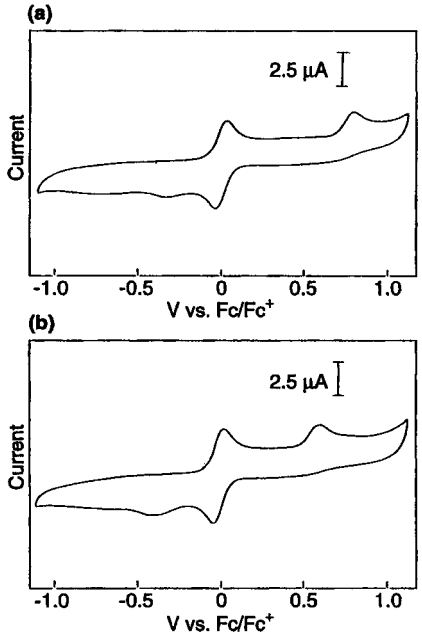

Figure 5. Cyclic voltammograms of (a) **1** and (b) **2** in MeCN: sample, 0.25 mM; supporting electrolyte, *n*-Bu_4NClO_4 (0.1 M); scan rate, 100 mV/s (central reversible redox peak is the voltammogram of ferrocene added as an internal standard).

TABLE 2: Oxidation (E^{ox}) and Reduction Peak Potentials (E^{red}) [V vs Fc/Fc^+] of 1 and 2[a]

compd	E_1^{ox}	E_1^{red}	E_2^{red}
1	+0.78	−0.32	−0.74
2	+0.61	−0.40	−0.75

[a] With 0.1 M *n*-Bu_4NCl_4 in MeCN at 298 K; sweep rate 100 mVs^{-1}.

error, which strongly suggests that the weak absorption bands corresponds not to the $S_0 \rightarrow T_1$ transition but to the $S_0 \rightarrow S_1$ transition.

Emission Spectra. The fluorescence spectra of **1** and **2** in a methanol/ethanol mixture (1:1) at 77 K indicated only one broad band with a peak at 453 and 502 nm, respectively, while phosphorescence bands were not observed. The fluorescence of **2** shifted to a longer wavelength region than that of **1**. The shape of each fluorescence band of **1** and **2** with excitation at 270 nm was almost identical with that with excitation at the corresponding lowest-energy absorption wavelength, 350 nm for **1** and 403 nm for **2**. The red shift of the fluorescence maximum for **2** is consistent with that of the lowest-energy absorption maximum for **2**. Moreover, excitation spectra concerning each fluorescence maximum of **1** and **2** showed two peaks, 270 and 350 nm for **1** and 283 and 410 nm for **2**. Thus, it is concluded that the absorption band at 350 nm for **1** (and also 403 nm for **2**) corresponds to the $S_0 \rightarrow S_1$ transition in accordance with the above absorption spectra.

Electrochemical Properties. To obtain further information about the electronic structures of **1** and **2**, the redox properties were examined on the basis of the CV measurements. The cyclic voltammograms and the redox potentials of **1** and **2** are shown in Figure 5 and Table 2, respectively. Both **1** and **2** had one oxidation peak and two reduction peaks, and all of the redox steps were irreversible. The first reduction potentials for **1** and **2** were similar to each other, indicating that the LUMO of both molecules lies at approximately the same energy level. The reduction potential of **1** was 0.08 V lower than that of **2**. On the other hand, the oxidation potentials showed a large difference

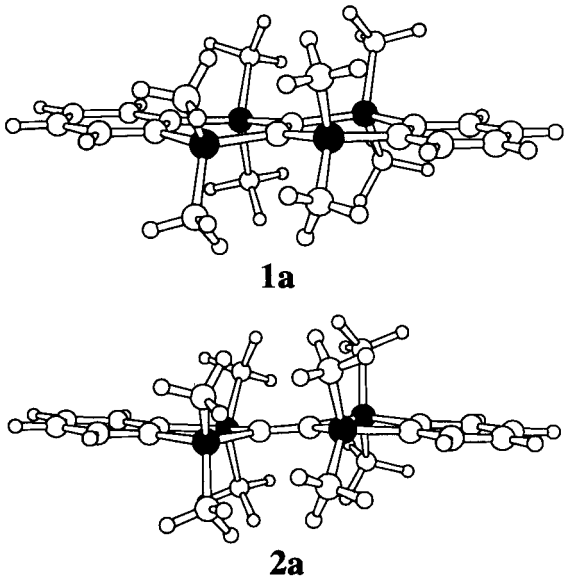

Figure 6. Overviews of the AM1 optimized structures of (a) **1a** and (b) **2a**.

TABLE 3: Optimized Bond Lengths (Å) and Angles (deg) of the Model Compounds 1a−2b

	AM1		RHF/6-31G*	
	1a	**2a**	**1b**	**2b**
	Bond Lengths			
C1−C2	1.324	1.317	1.361	1.354
Si1−C1	1.860	1.838	1.917	1.925
Si1−C3	1.787	1.793	1.877	1.882
C3−C4	1.388	1.395	1.330	1.334
C4−C5	1.397	1.390		
C5−C6	1.393	1.398		
C6−C7	1.396	1.394		
	Bond Angles			
Si1−C1−C2	122.6	128.3	122.5	127.9
C1−Si1−C3	114.0	103.3	110.7	99.5
Si1−C3−C4	122.9	114.5	123.8	116.9
Si1−C1−Si2	114.7	103.3		104.0
Si1−C3−C8	117.4	125.4		
C4−C3−C8	119.7	120.1		
C3−C8−C7	120.7	119.9		
C6−C7−C8	119.6	120.0		

of 0.17 V: +0.78 V for **1** and +0.61 V for **2** vs Fc/Fc^+. This result indicates that the HOMO of **2** is higher in energy than that of **1**. The fact that the HOMO−LUMO gap of **2** is smaller than that of **1** is in agreement with the observed bathochromic shift of the low-energy transition in the absorption spectra.

Optimized Geometries. The selected optimized bond lengths and angles of the model compounds **1a**, **2a** **1b**, and **2b** are listed in Table 3. The atoms in these compounds are labeled in Figure 3. The overviews of the AM1 optimized geometries of **1a** and **2a** are shown in Figure 6. Although both **1a** and **2a** take a shallow chair conformation with C_1 symmetry, each central tetrasilylethene moiety is planar; the dihedral angle between the peripheral benzene ring and the tetrasilylethene plane was 8.1° for **1** [10.1° for **2**]. The optimal C(1)═C(2) and Si(1)−C(1) distances of **1a**(**2a**) are 1.324(1.317) Å and 1.860(1.838) Å, respectively, being slightly shorter than the experimental values[2d,3] of 1.367−1.37 and 1.884−1.92 Å for the compounds having the planar tetrasilylethene moiety. It is noteworthy that the bond angles of Si(1)−C(1)−Si(2) were estimated to be 114.7° for **1a** and 103.3° for **2a**. Although the experimental value of the compounds related to **1** is so far unknown, the optimal value of **2a** is almost the same as the experimental value of the related compound 2,2,2′,2′-octamethyl-2,2′,5,5′-tetrasilabicyclopentylidene (104.5°).[3c] The optimal angle of **1a** agrees well with that (114°) of tetrakis(dimethylsilyl)ethene,[2d] suggesting that **1** has a less strained structure than **2**.

TABLE 4: INDO/S-CI Calculation Results of $S_0 \rightarrow S_n$ Transitions for 1a and 2a: Absorption Wavelengths λ (nm), Oscillator Strengths *f*, and Transition Moment Directions

	state	λ	*f*	transition moment direction
1a	2^1A_g	350	forbidden	
	1^1B_u	265	0.004	*y*
	2^1B_u	259	0.012	*y*
	1^1A_u	255	0.0005	*z*
	2^1A_u	218	0.057	*z*
	3^1B_u	207	1.73	*y*
2a	1^1B_g	367	forbidden	
	1^1B_u	264	0.010	*y*
	2^1B_u	241	0.013	*x*
	1^1A_u	239	0.00004	*z*
	3^1B_u	224	0.064	*y*
	2^1A_u	219	0.009	*z*
	3^1A_u	216	0.165	*z*
	4^1B_u	206	2.29	*y*

For the model compounds **1b** and **2b**, the geometry optimizations were performed at the RHF/6-31G* level. The optimized structures of **1b** and **2b** are of the chair conformation like **1a** and **2a**. However, both **1b** and **2b** have C_{2h} symmetry. The optimal C(1)═C(2) and Si(1)−C(1) distances of **1b**(**2b**) are 1.361(1.354) and 1.917(1.925) Å, respectively, being close to the above-mentioned experimental values. The peripheral C(3)═C(4) distance (1.330 Å for **1b** and 1.334 Å for **2b**) decreases from the central C(1)═C(2) bond. In the bond angle of Si(1)−C(1)−Si(2), close agreement is seen between the RHF/6-31G* (115.0° for **1b** and 104.0° for **2b**) and the AM1 values.

Assignment of the Absorption Spectra. In Table 4 are shown the results of assignment of the observed transitions of **1** and **2** based on the semiempirical SECI calculations for the AM1 optimized structures of **1a** and **2a**. A local C_{2h} symmetry was assumed here for **1a** and **2a**, ignoring the substituted methyl groups for simplicity.

The weak bands in the absorption spectra shown in Figure 4 are assigned as the HOMO (σ) → (LU+4)MO (π^*) excitation, the calculated absorption wavelengths being 350 nm for **1a** and 367 nm for **2a**. Although this type of transition (2^1A_g for **1** and 1^1B_g for **2**) is orbital-symmetry-forbidden, **1** and **2** could have finite oscillator strength owing to the deviation from the C_{2h} structures by random conformation of the ethyl groups. Although it is apparent from our emission spectral studies that the absorption band at 350 nm for **1** (and 403 nm for **2**) corresponds to the $S_0 \rightarrow S_1$ transition, we may note that the absorption wavelength corresponding to the $S_0 \rightarrow T_1$ transition was computed to be 379 and 400 nm for the model compounds **1a** and **2a**, respectively.

Higher-energy absorption bands observed in the range less than 300 nm differ in **1** and **2**. In **1**, two shoulders at 278 and 271 nm probably correspond to the two ^1B_u states with close absorption wavelengths (265 and 259 nm). The third shoulder of **1** observed at 237 nm is the most intense and can be interpreted by the 2^1A_u state at 218 nm with an oscillator strength of 0.057. This state is mainly composed of the (HO-2)MO → (LU+3)MO (57%) excitation. This transition is of $\pi-\pi^*$ type of the peripheral benzenes. The 3^1B_u state calculated at 207 nm with an oscillator strength of 1.73 was not observable in the UV−vis spectrum of **1**.

On the other hand, in **2**, two shoulders at 280 and 272 nm probably correspond to the two ^1B_u states with close absorption

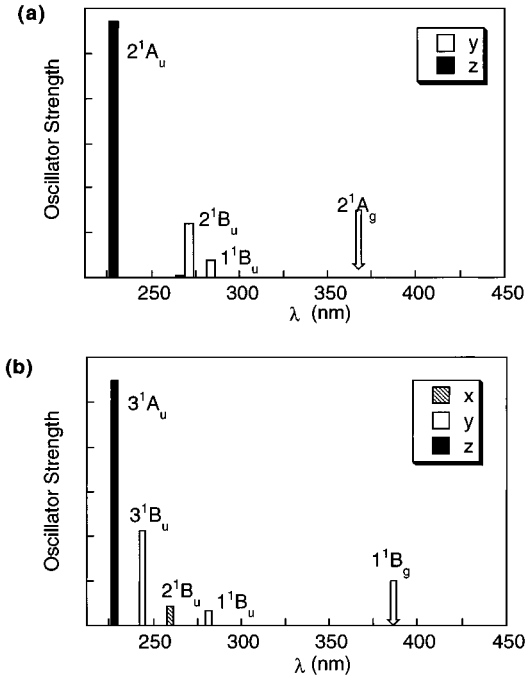

Figure 7. Graphical representation of the calculated transitions of **1a** and **2a**.

TABLE 5: CIS/6-31G* (INDO/S-CI[a]) Calculation Results of $S_0 \rightarrow S_n$ Transitions for 1b and 2b: Absorption Wavelengths λ (nm), Oscillator Strengths *f*, and Transition Moment Directions

model no.	state	λ	*f*	transition moment direction
1b	2^1A_g	269 (344)	forbidden	
	1^1A_u	197 (214)	0.094 (0.063)	*z*
	1^1B_u	186 (242)	0.030 (0.025)	*y*
2b	1^1B_g	286 (368)	forbidden	
	1^1B_u	192 (218)	0.72 (0.026)	*y*
	2^1B_u	179 (228)	0.015 (0.023)	*x*

[a] Geometrical parameters optimized by the MNDO AM1 method were used.

wavelengths (264 and 241 nm). The third shoulder of **2** observed at 258 nm probably corresponds to the 3^1B_u state. The peak observed at 235 nm is the most intense and can be interpreted as the 2^1A_u and 3^1A_u states at 219 and 216 nm with oscillator strengths of 0.009 and 0.165, respectively. The 4^1B_u state with the largest oscillator strength of 2.29 was not observable in the spectrum like the 3^1B_u state of **1a**.

For a more explicit comparison between experimental and theoretical spectra, the calculated $S_0 \rightarrow S_n$ transitions are depicted schematically in Figure 7. The absorption wavelengths in Figure 7 are uniformly corrected by adding 20 nm to the theoretical ones, since they are, on the average, 20 nm shorter than experimental values. The results of calculations are in satisfactory agreement with the experimental spectra.

Origin of the Bathochromic Shift in the $S_0 \rightarrow S_1$ Transition. In this section, we discuss the origin of the bathochromic shift in the $S_0 \rightarrow S_1$ transition of compounds **1** and **2**, employing the results of ab initio calculations at the CIS/6-31G* level with respect to the RHF/6-31G* optimized structures of simplified model compounds **1b** and **2b**. Table 5 lists the calculation results for the **1b** and **2b**. For comparison, the semiempirical SECI calculation results are also listed in Table 5. The lowest 2^1A_g state for **1b** [1^1B_g for **2b**] is described as the HOMO (σ) $\rightarrow$ LUMO (π^*) transition (42%) [46%], and the corresponding

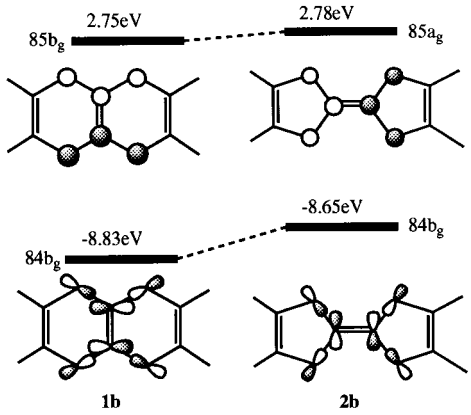

Figure 8. Relative energy levels of the HOMO and LUMO for the model compounds **1b** and **2b** based on the RHF/6-31G* calculations.

absorption wavelengths of **1b** and **2b** are 269 and 286 nm, respectively. Such a transition is one-photon-forbidden by the symmetry consideration as described in the previous section. The HOMO and LUMO patterns of **1b** and **2b** in Figure 8 show characteristics similar to those of the tetrasilylated ethylene in Figure 1. It should be noted that the calculated excitation energy to the 1^1A_u state for **1b** [1^1B_u state for **2b**] does not correspond to the actual absorption bands, since the calculated transition does not contain any contribution from benzene rings such as **1a** and **2a**. From these findings, there is considerable validity to the explanation of the origin of the bathochromic shift in question on the basis of the ab initio HF results of these model compounds.

The analysis of the SCF orbital energies indicates that the HOMO of **2b** lies 0.18 eV higher than that of **1b**. The main reason for this destabilization is that the small Si(1)−C(1)−Si(2) bond angle of **2b** causes both a decrease in the Si−C σ-bonding character and an increase in the out-of-phase overlapping between Si(1)−C(1) and Si(2)−C(1) bonding orbitals, as is clear from Figure 8. On the other hand, the energy difference between the LUMOs of **1b** and **2b** is small (0.03 eV). These results are consistent with those obtained by the CV measurements for **1** and **2**. The destabilization of the HOMO of **2b** consequently leads to a red shift of the $S_0 \rightarrow S_1$ transition in comparison with **1b**, which can be associated with a considerable bathochromic shift in the $S_0 \rightarrow S_1$ transition of **2** compared with **1**.

Conclusion

We have studied electronic structures of the two structural isomers of novel tetrasilyl-substituted ethylenes **1** and **2**. The UV−vis absorption spectra showed a weak absorption band in the range larger than 350 nm. From both the emission spectroscopic measurements and the INDO/S-CI calculations for the model compounds **1a** and **2a**, it has been concluded that the transition corresponds not to the spin-forbidden $S_0 \rightarrow T_1$ but to the symmetrically forbidden $S_0 \rightarrow S_1$ transition. Moreover, **2** showed a 57 nm bathochromic shift with respect to this weak band compared with **1**. This shift has been ascribed to raising the HOMO (σ) energy because of the small Si−C−Si bond angle of **2** by the ab initio calculations of the simplified model compounds **1b** and **2b**. The points made in this study would be common in principle to any tetrasilyl-substituted ethylenes. As described in the introduction of this paper, it is interesting to investigate the electronic properties of one-dimensional polymeric systems in Figure 2. Extension to those intriguing oligomers and/or polymers is now in progress.

Acknowledgment. This work is a part of the project of Institute for Fundamental Chemistry, supported by Japan Society for the Promotion of Science—Research for the Future Program (JSPS-RFTF96P00206). Numerical calculations were carried out at the Supercomputer Laboratory of the Institute for Chemical Research of Kyoto University.

References and Notes

(1) (a) Sakurai, H.; Kumada, M. *Bull. Chem. Soc. Jpn.* **1964**, *37*, 1894. (b) Sakurai, H. *J. Organomet. Chem.* **1980**, *200*, 261. (c) Bock, H. *Angew. Chem., Int. Ed. Engl.* **1989**, *28*, 1627.

(2) (a) Sakurai, H.; Nakadaira, Y.; Tobita, H.; Ito, T.; Toriumi, K.; Ito, H. *J. Am. Chem. Soc.* **1982**, *104*, 300. (b) Sakurai, H.; Tobita, H.; Nakadaira, Y.; Kabuto, C. *J. Am. Chem. Soc.* **1982**, *104*, 4288. (c) Sakurai, H.; Ebata, K.; Kabuto, C.; Nakadaira, Y. *Chem. Lett.* **1987**, 301. (d) Sakurai, H.; Ebata, K.; Sakamoto, K.; Nakadaira, Y.; Kabuto, C. *Chem. Lett.* **1988**, 965.

(3) Murakami, M.; Suginome, M.; Fujimoto, K.; Ito, Y. *Angew. Chem., Int. Ed. Engl.* **1993**, *32*, 1473. (b) Sekiguchi, A.; Ichinohe, M.; Kabuto, C.; Sakurai, H. *Organometallics* **1995**, *14*, 1092. (c) Sekiguchi, A.; Ichinohe, M.; Kabuto, C.; Sakurai, H. *Bull. Chem. Soc. Jpn.* **1995**, *68*, 2981.

(4) Hibino, J.; Nakatsukasa, S.; Fugami, K.; Matsubara, S.; Ohshima, K.; Nozaki, H. *J. Am. Chem. Soc.* **1985**, *107*, 6416.

(5) Ito, A.; Yoshii, T.; Tanaka, K. Unpublished work.

(6) Naka, A.; Hayashi, M.; Okazaki, S.; Kunai, A.; Ishikawa, M. *Organometallics* **1996**, *15*, 1101.

(7) Dewar, M. J. S.; Zoebisch, E. G.; Healy, E. F.; Stewart, J. J. P. *J. Am. Chem. Soc.* **1985**, *107*, 3902.

(8) Ridley, J. E.; Zerner, M. C. *Theor. Chim. Acta* **1973**, *32*, 111.

(9) (a) Bene, J. D.; Jaffé, H. H. *J. Chem. Phys.* **1968**, *48*, 1807. (b) Bene, J. D.; Jaffé, H. H. *J. Chem. Phys.* **1968**, *48*, 4050.

(10) Pierce, B. M. *J. Chem. Phys.* **1989**, *91*, 791.

(11) Nishimoto, K.; Mataga, N. *Z. Phys. Chem.* **1957**, *12*, 335.

(12) Hehre, W. J.; Radom, L.; Schleyer, P. v. R.; Pople, J. A. *Ab Initio Molecular Orbital Theory*; Wiley: New York, 1986.

(13) Dobosh, P. A. *QCPE* **1969**, *11*, 141.

(14) Frisch, M. J.; Trucks, G. W.; Schlegel, H. B.; Gill, P. M. W.; Johnson, B. G.; Robb, M. A.; Cheeseman, J. R.; Keith, T.; Peterson, G. A.; Montgomery, J. A.; Raghavachari, K.; Al-Laham, M. A.; Zakrzewski, V. G.; Ortiz, J. V.; Foresman, J. B.; Cioslowski, J.; Stefanov, B. B.; Nanayakkara, A.; Challacombe, M.; Peng, C. Y.; Ayala, P. Y.; Chen, W.; Wong, M. W.; Andres, J. L.; Replogle, E. S.; Gomperts, R.; Martin, R. L.; Fox, D. J. Binkley, J. S.; Defrees, D. J.; Baker, J.; Stewart, J. P.; Head-Gordon, M.; Gonzalez, C.; Pople, J. A. *Gaussian 94*, revision, D.4; Gaussian, Inc.: Pittsburgh, PA, 1995.

(15) McGlynn, S. P.; Azumi, T.; Kinoshita, M. *Molecular Spectroscopy of the Triplet State*; Prentice Hall: NJ, 1969.